Adsorption of Ni^{2+} from aqueous solution by magnetic Fe@graphite nano-composite

Wojciech Konicki[1,*], Rafał Pelka[2], Walerian Arabczyk[2]

[1]*Maritime University of Szczecin, Department of Integrated Transport Technology and Environmental Protection, Henryka Poboznego St. 11, 70-507 Szczecin, Poland*
[2]*West Pomeranian University of Technology, Szczecin, Institute of Chemical and Environment Engineering, Pułaskiego St. 10, 70-322 Szczecin, Poland*
[*]*Corresponding author: e-mail: w.konicki@am.szczecin.pl*

The removal of Ni^{2+} from aqueous solution by iron nanoparticles encapsulated by graphitic layers (Fe@G) was investigated. Nanoparticles Fe@G were prepared by chemical vapor deposition CVD process using methane as a carbon source and nanocrystalline iron. The properties of Fe@G were characterized by X-ray Diffraction method (XRD), High-Resolution Transmission Electron Microscopy (HRTEM), Fourier Transform-Infrared Spectroscopy (FTIR), BET surface area and zeta potential measurements. The effects of initial Ni^{2+} concentration (1–20 mg L^{-1}), pH (4–11) and temperature (20–60ºC) on adsorption capacity were studied. The adsorption capacity at equilibrium increased from 2.96 to 8.78 mg g^{-1}, with the increase in the initial concentration of Ni^{2+} from 1 to 20 mg L^{-1} at pH 7.0 and 20ºC. The experimental results indicated that the maximum Ni^{2+} removal could be attained at a solution pH of 8.2 and the adsorption capacity obtained was 9.33 mg g^{-1}. The experimental data fitted well with the Langmuir model with a monolayer adsorption capacity of 9.20 mg g^{-1}. The adsorption kinetics was found to follow pseudo-second-order kinetic model. Thermodynamics parameters, ΔHO, ΔGO and ΔSO, were calculated, indicating that the adsorption of Ni^{2+} onto Fe@G was spontaneous and endothermic in nature.

Keywords: magnetic nanocomposite, iron nanoparticles, nickel, adsorption.

INTRODUCTION

Heavy metals belong to one of the most serious environment pollutants today. Unlike organic contaminants, heavy metals are not biodegradable and can lead to accumulation in living organisms, causing various diseases and disorders. Therefore, in recent years, many investigations have focused on the removal of heavy metals from water[1–8]. One of the more important toxic heavy metals present in water and wastewaters is nickel. It is widely used in a wide variety of industries such as metal plating and cadmium-nickel battery, galvanizing, smelting, mining, pigments, stabilizers and alloys. The nickel salts are known to be acutely and chronically toxic to human. Acute poisoning of Ni^{2+} causes headache, dizziness, nausea, and tightness of the chest, chest pain, shortness of breath, dry cough, cyanosis, and extreme weakness. At higher concentrations it is a potent carcinogen and causes cancer of lungs, nose and bone[9]. Therefore, it becomes essential to remove the nickel ions from wastewaters. A number of specialized processes have been developed for the removal of Ni^{2+} from water and waste discharges. These unit operations include: flotation[10], filtration[11], photocatalytic removal[12], electrochemical operation[13], ion-exchange[14], complexation[15] and co-precipitation[16].

As an economical and efficient method, adsorption technique has been widely applied to remove heavy metal ions from wastewaters. To date, numerous adsorbents, such as spent animal bones[17], crab shell[18], seaweeds[19], nanoparticle Fe$_3$O$_4$ impregnated onto tea waste[20], activated carbon[21], olive stone waste[22], fly ash[23], powdered egg shell[24], coconut husk[25] and carbon nanotubes[26–29], have been examined for their ability to remove of Ni^{2+} from aqueous solutions.

The important aspect in the adsorption process is the separation of the adsorbent from the aqueous solution. Compared with traditional centrifugation and filtration methods, the magnetic separation method is considered as a rapid, relatively simple and effective technique for separating adsorbents from aqueous solutions. So far, several methods have been developed to prepare the magnetic carbon nanocomposites as adsorbents for the removal of pollutants from water. Wu et al. have synthesized magnetic Fe$_3$O$_4$@C nanocomposite via a facile one-step solvothermal process using ferrocene as both iron and carbon resource in the presence of hydrogen peroxide[30]. He et al. reported a two-step process to fabricate hybrids of graphene oxide GO nanosheets and surface-modified Fe$_3$O$_4$ nanoparticles[31]. Hao et al. have prepared magnetic graphene oxide nanocomposite GO-Fe$_3$O$_4$ by chemical co-precipitation of Fe^{2+} and Fe^{3+} in alkaline solution in the presence of GO for removal of Chrysoidine Y[32]. Qu et al. have synthesized multi-walled carbon nanotubes filled with Fe$_2$O$_3$ particles via wet chemical method for removal of Methylene Blue and Neutral Red[33]. Zhu et al. have synthesized magnetic carbon nanocomposite by microwave assisted heating as the magnetic adsorbent for the removal of Cr^{6+} [34].

In the present work, we prepared magnetic Fe@G nanocomposite by a simple CVD method for the removal of Ni^{2+} from aqueous solution. The effects of pH, temperature and initial dye concentration on Ni^{2+} adsorption by the Fe@G were investigated. The experimental data were analyzed using the pseudo-first-order and the pseudo-second-order kinetic model. Langmuir and Freundlich isotherms were employed to quantify the adsorption equilibrium. Thermodynamics parameters, ΔG^o, ΔH^o and ΔS^o, were also calculated.

EXPERIMENTAL

Material and characterization methods

Analytical grade nickel standard solution (Ion Standard Solution of 1000 mg L^{-1}) was purchased from Merck and was employed to prepare stock solution containing 100 mg L^{-1} of Ni^{2+}. The stock solution was then further diluted to the desired concentrations. Dimethylglyoxime was obtained from Fluka.

Fe@G was obtained by chemical vapor deposition CVD process using methane as a carbon source and nanocrystalline iron. The synthesis was conducted in the flow tubular reactor with thermogravimetric measurement of mass changes. Nanocrystalline iron was obtained by fusion of magnetite with small amounts of promoter oxides (Al$_2$O$_3$, K$_2$O and CaO), followed by reduction with hydrogen. Details of the nanocrystalline iron preparation are given in work[35]. The nanocrystalline iron was placed in the platinum basket and in the first stage was reduced polythermally by hydrogen with the rate of 15°C/min. In the second stage, the synthesis of nanocomposite was performed by carburization of nanocrystalline iron by methane under atmospheric pressure at 650°C. The process was carried out to the carburization degree n$_C$/n$_{Fe}$ = 19, where n$_C$/n$_{Fe}$ is the ratio of the numer of carbon moles to iron moles in the carbon-iron system. Afterwards the sample was cooled to the room temperature under methane atmosphere.

The phase composition of the Fe@G was determined using the X-ray diffraction method (X'Pert PRO Philips diffractometer) using a CuKα radiation. The morphology of the adsorbent was investigated by high-resolution transmission electron microscopy HRTEM using a FEI Tecnai F20. The Fe@G was analyzed for their BET-specific surface area and pore-size distribution using an Quadrasorb SI Quantachrome analyzer. The functional groups on the Fe@G surface were determined using fourier transform infrared FTIR method (Nicolet iS5 FT-IR Spectrometer, Thermo Scientific). The zeta potential of sample was determined by a Malvern Instrument Zetasizer 2000 at room temperature. All solutions were prepared with deionized water.

Adsorption experiments

Adsorption experiments were carried out in Erlenmeyer flask, where the solution (150 mL) with initial Ni^{2+} concentration was placed. Initial concentrations of Ni^{2+} were varied from 1 to 20 mg L^{-1}. The flask with Ni^{2+} solution was sealed and placed in a temperature controlled shaking water bath (Grant OLS26 Aqua Pro, Grant Instruments Ltd) and agitated at a constant speed of 160 rpm. To observe the effect of temperature the experiments were carried out at three different temperatures, i.e., 20, 40 and 60°C. Before mixing with the adsorbent, various pH levels of the solution was adjusted by adding a few drops of diluted hydrochloric acid (0.1 N HCl) or sodium hydroxide (0.1 N NaOH). When the desired temperature was reached, about 40 mg of Fe@G was added into flask. At the end of the equilibrium period 1 ml of aqueous sample was taken from the solution, and the liquid was separated from the adsorbent magnetically. The determination of Ni^{2+} concentration was done spectrophotometrically (GE-

NESYS 10S UV-VIS Spectrometer, Thermo Scientific) at 530 nm using the dimethylglyoxime method[36]. The amount of Ni^{2+} adsorbed at equilibrium qe (mg g^{-1}) was calculated by following equation:

$$q_e = \frac{(C_0 - C_e)V}{m} \qquad (1)$$

where C$_0$ (mg L^{-1}) is the initial Ni^{2+} concentration, C$_e$ (mg L^{-1}) the Ni^{2+} concentration at equilibrium, V (L) the volume of the solution and m (g) is the mass of the adsorbent.

The procedures of kinetic experiments were identical with those of equilibrium tests. At predetermined moments, aqueous samples were taken from the solution, the liquid was separated from the adsorbent and concentration of Ni^{2+} in solution was determined spectrophotometrically. The amount of Ni^{2+} adsorbed at time t q$_t$ (mg g^{-1}) was calculated by following equation:

$$q_t = \frac{(C_0 - C_t)V}{m} \qquad (2)$$

where C$_t$ (mg L^{-1}) the Ni^{2+} concentration at any time t. Each experiment was carried out in duplicate and the average results are presented. The kinetic and isotherm models were evaluated by the linear correlation coefficient (R^2).

RESULTS AND DISCUSSION

Characterization of the adsorbent

Figure 1 shows the X-ray diffraction pattern of Fe@G. The diffraction peak at 2θ = 26.2° corresponds to the (002) hexagonal planes of crystalline graphite. The peaks at around 44.6°, 65.1°, and 82.4° can be indexed as (110), (200), and (211) diffraction planes of α-Fe. Additionally, small amount of iron carbide Fe$_3$C phase was detected using the reference standard JCPDS file 35-0772 (Not marked peaks). The morphological structure of Fe@G is shown in Figure 2. It can be seen that the nanoparticles are composed of a metallic iron core and a carbon shell. Figure 2 also reveals that the sheets are well graphitized and the interlayer spacing of the shell is about 0.34 nm, which is consistent with the d value of (002) plane of hexagonal graphite[37]. Taking into account that the iron at room temperature is ferromagnetic, Fe@G nanocomposite was easily removable from aqueous solution by external magnetic field (Fig. 3). Figure 4 shows an EDX spectrum of Fe@G which reveals the presence of carbon from the shell and iron. The Cu peaks were from the copper grid. The BET surface area was found
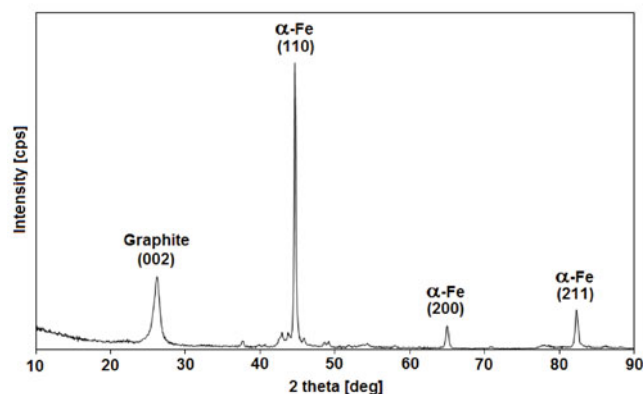

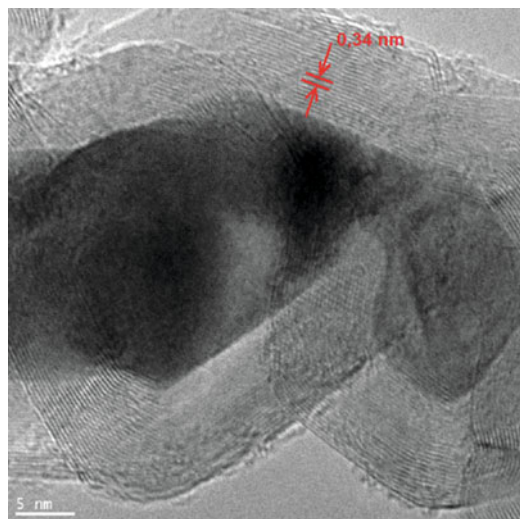**Figure 1.** X-ray diffraction pattern of Fe@G

Figure 2. HRTEM image of Fe@G particles

to be 47 m^2 g^{-1}, the total pore volume was 17.7 cm^3 g^{-1} and the pore radius was 0.016 nm. Figure 5 shows the FTIR spectrum of Fe@G. The broad peak at 1080 cm^{-1} can be assigned to C-O stretching vibrations in ethers, alcohols, anhydrides, lactones or carboxylic acids[38]. The peak at 1380 cm^{-1} corresponds to O-H bending vibrations in carboxyl groups (COOH)[39]. The peak at 1629 cm^{-1} can be assigned to C=O groups in different environments (carboxylic acid, ketone/quinone) and to C=C in aromatic rings[40]. Two peaks at 2923 and 2848 cm^{-1} are a result of aliphatic asymmetric C-H stretching and symmetric C-H stretching vibrations in methylene group

Figure 3. Photograph of magnetic separation of Fe@G from the aqueous solution with a permanent magnet
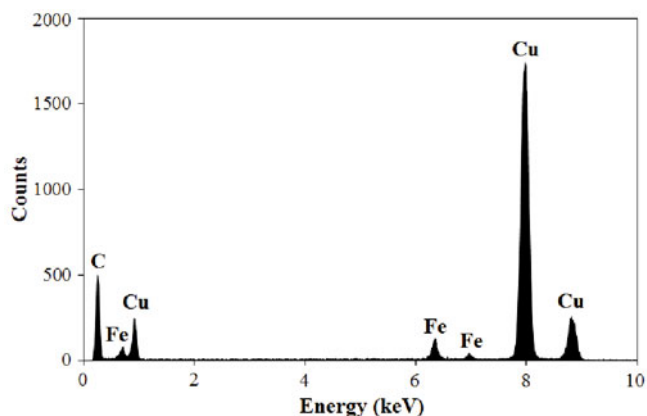

Figure 4. EDX spectrum of Fe@G

(CH$_2$), respectively[41]. The peak at 3440 cm^{-1} comes from the O-H stretching vibrations in adsorbed water[42]. The zeta potentials of Fe@G were measured in water solution at pH in the range 3.5–11.0, and decreased from positive to negative values with increasing pH over the whole studied range (Fig. 6).The pHpzc of Fe@G was found to be 7.70. More detailed analysis with Raman spectra and thermoprogrammable oxidation TPO profile is described elsewhere[43].
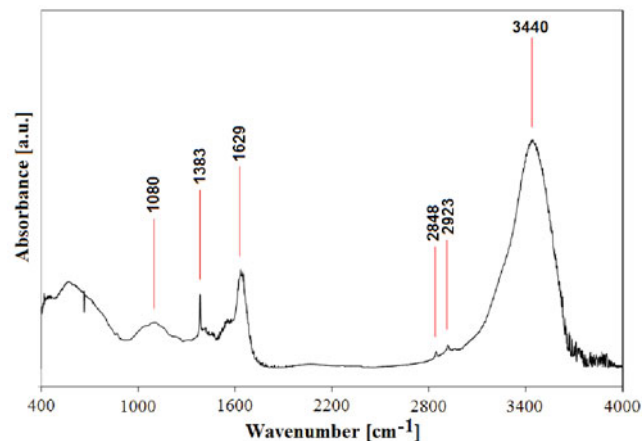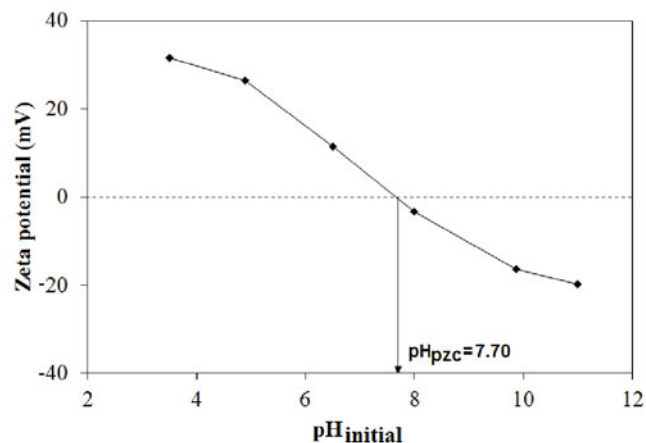

Figure 5. FTIR spectra of Fe@G

Figure 6. The effect of pH on zeta potential of Fe@G

Adsorption kinetics

The influence of initial concentration of Ni^{2+} on its adsorption onto Fe@G was investigated in the concentration range 1–20 mg L^{-1} at pH 7.0 and 20°C. The adsorption of the Ni^{2+} onto Fe@G increased with time and then attained equilibrium value at a time of about 2 h (Fig. 7). As seen in Figure 7, the adsorption capacity at equilibrium increased from 2.96 to 8.78 mg g^{-1}, with the increase in the initial concentration of Ni^{2+} from 1 to 20 mg L^{-1}.

In order to investigate the adsorption mechanism of Ni^{2+} onto Fe@G, two kinetic models, pseudo first-order and pseudo-second-order kinetic model, were tested to find the best fitted model for the experimental data. The pseudo-first-order model is represented by the following equation[44]:

$$\ln(q_e - q_t) = \ln q_e - k_1 t \tag{3}$$

where q_e (mg g^{-1}) is the amount of Ni^{2+} adsorbed per unit mass of adsorbent at equilibrium, q_t (mg g^{-1}) is the amount of Ni^{2+} adsorbed per unit mass of adsorbent at any time t (min) and k_1 (min^{-1}) is the first-order rate
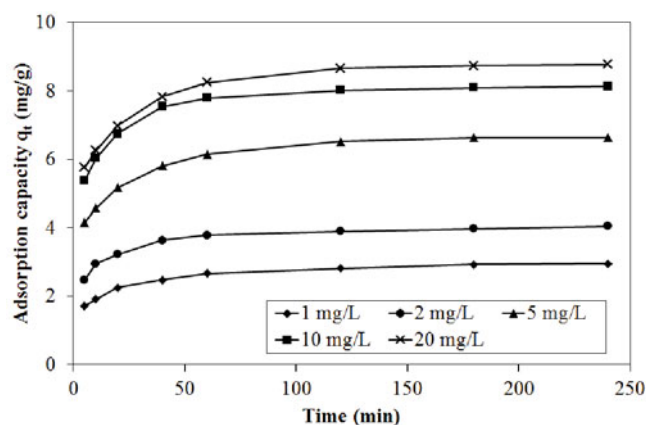
Figure 7. The effect of initial concentration of Ni2+ on adsorption capacity onto Fe@G (Experimental conditions: T = 20ºC, pH = 7)

constant adsorption. Values of k_1 and equilibrium adsorption density q_e at 20ºC were calculated from the plots of $\ln(q_e - q_t)$ versus t for different initial concentrations of Ni^{2+}. The pseudo-second-order kinetic model can be expressed as follows:

$$\frac{t}{q_t} = \frac{1}{k_2 q_e^2} + \frac{1}{q_e} t \tag{4}$$

where k_2 (g mg^{-1} min^{-1}) is the rate constant for the pseudo-second-order adsorption kinetics. Values of k_2 and q_e for different initial concentrations of Ni^{2+} were calculated from the slope and intercept of the linear plot of t/q_t versus t. The plot of t/q_t versus t at 20ºC, is shown in Figure 8. The results of the kinetic data are listed in Table 1. Based on the correlation coefficients, it can be said that the adsorption fits to the pseudo-second-order ($R^2 = 0.999 \div 1$) better than the pseudo-first-order kinetic model ($R^2 = 0.842 \div 0.951$). Additionally, the experimental adsorption capacity $q_{e,exp}$ values were very close to the calculated adsorption capacity $q_{e,cal}$ values, verifying the
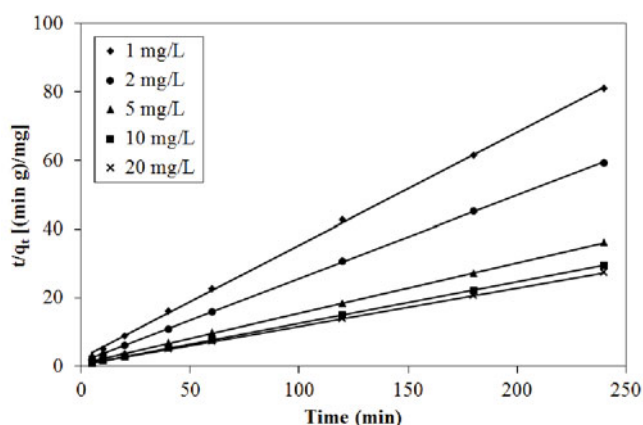
high correlation of adsorption to the pseudo-second-order model. These facts suggest that the pseudo-second-order adsorption mechanism is predominant. Similar kinetic behavior has also been reported in the literature[28, 45].

Adsorption isotherms

Adsorption isotherm models are fundamental in describing the interactive behavior between the adsorbate and adsorbents, and are important for investigating mechanisms of adsorption. Two well known models, namely the Langmuir and Freundlich models, were used to analyze the experimental data.

The Langmuir's isotherm model is represented by the following linear equation[46]:

$$\frac{C_e}{q_e} = \frac{1}{Q_0 b} + \frac{C_e}{Q_0} \tag{5}$$

where C_e (mg L^{-1}) is the equilibrium concentration of the adsorbate, q_e (mg g^{-1}) is the amount of adsorbate adsorbed per unit mass of adsorbent at equilibrium, Q_0 (mg g^{-1}) is the monolayer adsorption capacity and b (L mg^{-1}) is a constant related to energy of adsorption. The values of Q_0 and b were calculated from the slope and intercept of the linear plot C_e/q_e versus C_e. The plot of C_e/q_e versus C_e at 20ºC is shown in Figure 9a. The essential characteristics of the Langmuir isotherm can be expressed in terms of a dimensionless equilibrium parameter (R_L), which is defined by the following equation:

$$R_L = \frac{1}{1 + bC_0} \tag{6}$$

where b (L mg^{-1}) is the Langmuir constant and C_0 (mg L^{-1}) is the highest initial concentration of the adsorbate. The value of R_L indicates the type of the isotherm to be either unfavorable ($R_L > 1$), linear ($R_L = 1$), favorable ($0 < R_L < 1$) or irreversible ($R_L = 0$). The values of R_L was found to be 0.045 and confirmed that the MMWCNTs-C is favorable for adsorption of Ni^{2+} under the conditions used in this study.

The linear form of Freundlich equation can be expressed as follows:

$$\ln q_e = \ln K_e + \left(\frac{1}{n}\right) \ln C_e \tag{7}$$

where q_e (mg g^{-1}) is the amount of adsorbate adsorbed per unit mass of adsorbent at equilibrium, K_F (mg g^{-1}(L mg^{-1})$^{1/n}$) and n are Freundlich constants, which represent adsorption capacity and adsorption strength, respectively and C_e (mg L^{-1}) is the equilibrium concentration of the adsorbate. The values of K_F and n were calculated from the slope and intercept of the linear plot $\ln q_e$ versus $\ln C_e$ (Fig. 9b). The calculated Langmuir and Freundlich constants and their corresponding linear regression correlation coefficient values R^2 are given in Table 2. As

Figure 8. Pseudo-second-order kinetics of adsorption Ni^{2+} onto Fe@G at 20ºC

Table 1. Comparison of the pseudo-first-order and pseudo-second-order kinetic models for different initial concentrations of Ni^{2+} at 20ºC

C_o [mg · L^{-1}]	$q_{e,exp}$ [mg · g^{-1}]	Pseudo-first-order kinetic model			Pseudo-second-order kinetic model		
		k_1 [min^{-1}]	$q_{e,cal}$ [mg · g^{-1}]	R^2	k_2 [g · mg^{-1} · min^{-1}]	$q_{e,cal}$ [mg · g^{-1}]	R^2
1	2.96	0.0206	1.43	0.935	0.0482	3.03	0.999
2	4.05	0.0187	1.49	0.842	0.0518	4.10	0.999
5	6.64	0.0298	3.32	0.934	0.0279	6.80	0.999
10	8.14	0.0264	2.93	0.915	0.0335	8.26	1
20	8.78	0.0274	3.73	0.951	0.0247	8.95	0.999

Figure 10. The effect of initial pH solution on adsorption Ni^{2+} onto Fe@G (Experimental conditions: $C_{Ni^{2+}}^{O}$ = 10 mg L^{-1}, T = 20°C)

is presents in the species of Ni^{2+}, $Ni(OH)^{+}$, $Ni(OH)_2$, $Ni(OH)_3^{-}$ and $Ni(OH)_4^{2-}$ at different pH values[28]. At pH<9, the predominant specie is Ni^{2+}. With an increase in pH, the concentration of Ni^{2+} ions decreases rapidly and increases the concentration of $Ni(OH)^{+}$, $Ni(OH)_2$ and $Ni(OH)_3^{-}$. Therefore, the adsorption of Ni^{2+} onto Fe@G surface is lower at higher pH.

Effect of temperature

The effect of temperature on equilibrium adsorption of Ni^{2+} onto Fe@G was studied for three temperatures of 20, 40, and 60°C, at 10 mg L^{-1} initial Ni^{2+} concentra-
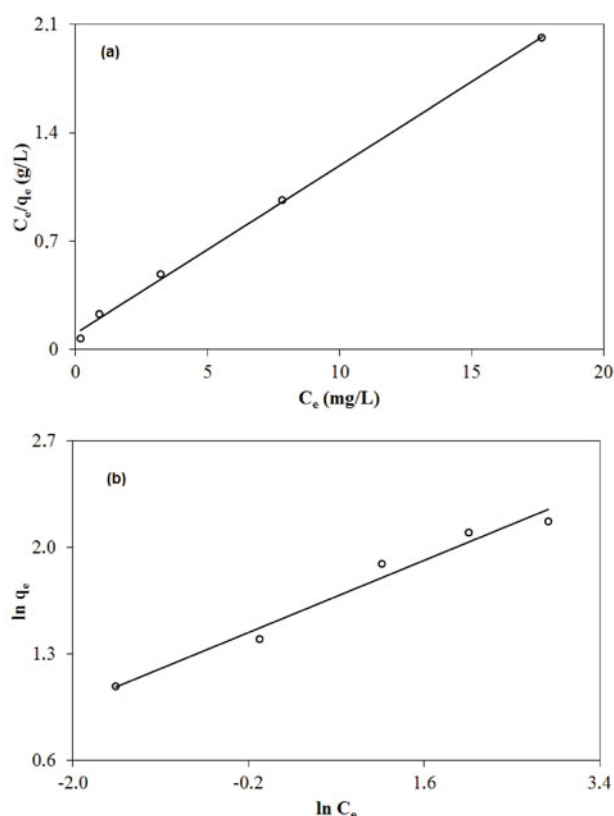
Figure 9. Langmuir (a) and Freundlich (b) adsorption isotherm of Ni^{2+} onto Fe@G at 20°C

seen, the experimental data better fit Langmuir model (R^2 = 0.998) than the Freundlich model (R^2 = 0.974). Additionally, it was observed that the maximum monolayer adsorption capacity Q_O of Fe@G for Ni^{2+} was found to be 9.20 mg g^{-1}. Table 3 lists and compares the maximum monolayer adsorption capacity of Ni^{2+} on various adsorbents.

Effect of pH

The effect of the initial pH on the adsorption capacity of Ni^{2+} is shown in Figure 10. As shown in Figure 10, with the pH value of the solution increased from 4.0 to 8.2, the adsorption capacity increased from 4.55 to 9.33 mg g^{-1}, and then decreased continuously from 9.33 to 5.81 mg g^{-1} with the increase of the pH from 8.2 to 11.0.

The pHpzc of Fe@G was found to be 7.70. At pH values lower than pHpzc the surface of Fe@G is positively charged. At acidic pH, carboxylic groups are protonated to the cationic form ($-COOH_2^{+}$) and repulsive interaction between the adsorbent surface and the nickel ions take place. As the pH increases, the numer of positively charged sites decreases and the numer of negatively charged sites increases. At pH>pHpzc carboxylic groups dissociate to anionic form ($-COO^{-}$), which increases the number of fixed ionized groups and generates electrostatic attraction force with Ni^{2+}. However, with further increasing pH from 8.2 to 11.0, the adsorption capacity of Ni^{2+} decreased. Decrease in adsorption capacity at higher pH is probably due to formation of soluble hydroxy complexes. Nickel
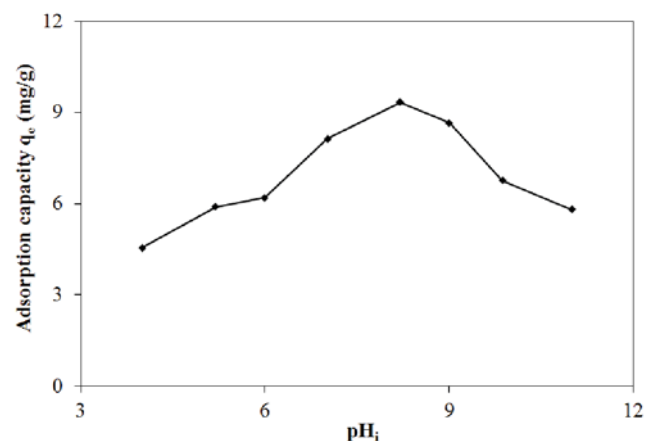
Table 3. Comparison of the maximum monolayer adsorption of Ni^{2+} on various adsorbents

Adsorbent	Q_O [mg · g^{-1}]	Ref.
Bagasse	0.001	23
Fly ash	0.03	23
Aspergillus niger	1.10	47
Oxidized CNTs	1.83	26
Oxidized MWCNTs	3.73	28
Rice hull	5.75	48
Sheep manure waste	7.20	49
Deactivated protanated yeast	9.01	50
Peat moss	9.18	51
Fe@G	9.20	This study
Coir pith	9.50	52
Calcium alginate	10.50	53
Fe_3O_4	11.53	54
Carbon aerogel	12.87	55
Zeolite/vermiculite composite	16.50	56
Activated carbon prepared from almond husk	30.77–37.18	21
Granular activated carbon	45.46–125.00	57
Graphene nanosheet/δ-MnO_2 [GNS/MnO_2] composite	46.55	58
Activated carbon-zeolite composite (type 2)	62.22	59
Activated carbon-zeolite composite (type 1)	70.43	59
Cajanus cajan L Milsp seed shells activated carbon	85.69–156.25	60
Lignocellulose/Montmorillonite nanocomposite	94.86	61

Table 2. Langmuir and Freundlich parameters for the adsorption of the Ni^{2+} on Fe@G at 20°C

Langmuir isotherm				Freundlich isotherm		
Q_O [mg · g^{-1}]	b [L · mg^{-1}]	R_L	R^2	K_F [(mg · g^{-1})(L · mg^{-1})$^{1/n}$]	n	R^2
9.20	1.06	0.045	0.998	4.46	3.79	0.974

tion and pH 7.0. As shown in Figure 11a, the adsorption capacity of Ni^{2+} increased at higher temperatures, which indicates that adsorption in this system was an endothermic process. The thermodynamic parameters such as enthalpy (ΔH^O), entropy (ΔS^O) and Gibbs free energy (ΔG^O), were determined by using the following equations[62]:

$$\ln K_a = \frac{\Delta S^o}{R} - \frac{\Delta H^o}{R \cdot T} \tag{8}$$

$$K_a = \frac{q_e}{C_e} \tag{9}$$

$$\Delta G^o = - RT \ln K_a \tag{10}$$

where T (K) is the solution temperature, K_a is the adsorption equilibrium constant, R (8.314 J mol^{-1} K^{-1}) is the gas constant. Enthalpy (ΔH^o) and entropy (ΔS^o) were calculated from the slope and intercept of van't Hoff plot of ln q_e/C_e versus 1/T (Fig. 11b). The value of Gibbs free energy (ΔG^o) was calculated using Eq. 10. The values of ΔH^o, ΔS^o and ΔG^o are listed in Table 4. The positive value of ΔH^o (3.21 kJ mol^{-1}) confirms the endothermic process, meaning the reaction consume energy. Kara et al. suggested that the ΔH^o of physisorption is smaller than 40 kJ mol^{-1} [63]. Thus, the values of

ΔH^O suggests that the adsorption of Ni^{2+} onto Fe@G is a physisorption process. Also, the positive value of ΔS^o (11.3 J mol^{-1} K^{-1}) suggest the increased randomness at the solid-solution interface during the adsorption of Ni^{2+} onto Fe@G. The values of Gibbs free energy (ΔG^o) were negative at all of the tested temperatures, confirming that the adsorption of Ni^{2+} onto Fe@G was spontaneous and thermodynamically favorable. The change in Gibbs free energy for physisorption is between –20 and 0 kJ mol^{-1}, the physisorption together with chemisorptions is at the range of –20 to –80 kJ mol^{-1} and chemisorption is at the range of –80 to –400 kJ mol^{-1} [64]. The values of ΔG^o for the adsorption of Ni^{2+} onto Fe@G were in the range of physisorption.

CONCLUSIONS

The adsorption of Ni^{2+} onto Fe@G from aqueous solutions was investigated under various conditions. The prepared adsorbent with the adsorbed pollutants can be easily separated by using an external magnetic field. The adsorption kinetics was best in accordance with the pseudo-second-order kinetic model. Langmuir isotherm was better to fit the experimental data compared with the Freundlich model. The monolayer adsorption capacity was found to be 9.20 mg g^{-1}. The thermodynamic parameters (ΔH^o, ΔG^o and ΔS^o) showed that the adsorption process of Ni^{2+} onto Fe@G was a spontaneous and endothermic process. Additionally, the values ΔH^O and ΔG^O suggested that the adsorption of Ni^{2+} onto Fe@G was a physisorption process.

ACKNOWLEDGEMENT

LITERATURE CITED

1. Gupta, V.K., Srivastava, S.K., Mohan, D. & Sharma, S. (1998). Design parameters for fixed bed reactors of activated carbon developed from fertilizer waste for the removal of some heavy metal ions. *Waste Manage.* 17(8), 517–522. DOI: 10.1016/S0956-053X(97)10062-9.

2. Gupta, V.K., Agarwal, S. & Saleh, T.A. (2011). Synthesis and characterization of alumina-coated carbon nanotubes and their application for lead removal, *J. Hazard. Mater.* 185(1), 17–23. DOI: 10.1016/j.jhazmat.2010.08.053.

3. Gupta, V.K. & Nayak, A. (2012). Cadmium removal and recovery from aqueous solutions by novel adsorbents prepared from orange peel and Fe_2O_3 nanoparticles. *Chem. Eng. J.* 180, 81–90. DOI: 10.1016/j.cej.2011.11.006.

4. Saleh, T.A. & Gupta, V.K. (2012). Column with CNT/magnesium oxide composite for lead(II) removal from water. *Environ. Sci. Pollut. Res.* 19(4), 1224–1228. DOI: 10.1007/s11356-011-0670-6.

5. Gupta, V.K., Nayak, A. & Agarwal, S. (2015). Bioadsorbents for remediation of heavy metals: Current status and
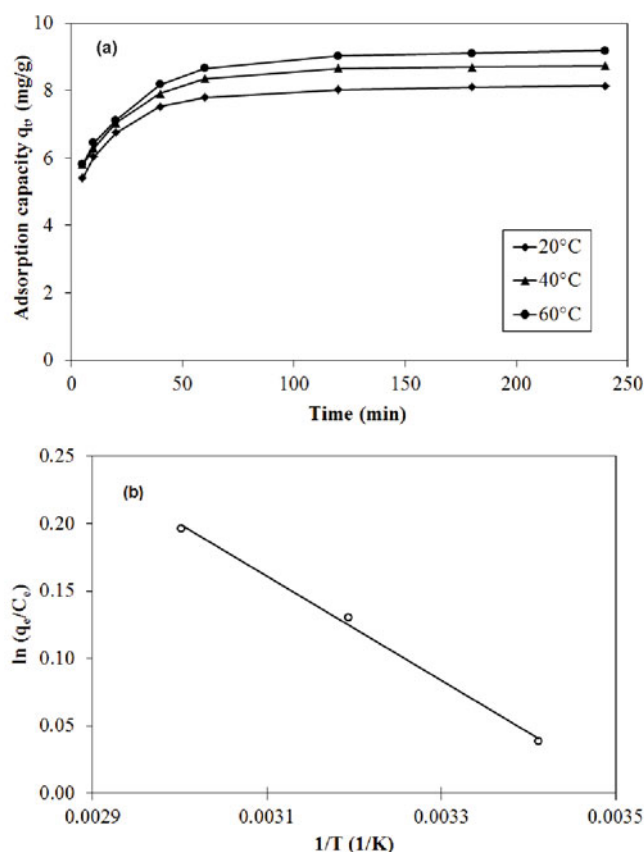
Figure 11. Effect of temperature on adsorption of the Ni2+ onto Fe@G. (Experimental conditions: $C^O_{Ni^{2+}}$ = 10 mg L^{-1}, pH = 7.0). (b) Van't Hoff plot for the adsorption of the Ni2+ onto Fe@G

Table 4. Thermodynamic parameters for the adsorption of the Ni^{2+} onto Fe@G

Ni^{2+} con- centration [mg · L^{-1}]	ΔH^O [kJ · mol^{-1}]	ΔS^O [J · mol^{-1} · K^{-1}]	ΔG^o at temperature [^{o}C] [J · mol^{-1}]		
			20	40	60
10	3.21	11.3	−93.3	−339.3	−543.7

their future prospects. *Environ. Eng. Res*. 20(1), 001–018. DOI: 10.4491/eer.2015.018.

6. Goswami, A., Raul, P.K. & Purkait, M.K. (2012). Arsenic adsorption using copper (II) oxide nanoparticles. *Chem. Eng. Res. Des*. 90, 1387–1396. DOI: 10.1016/j.cherd.2011.12.006.

7. Khan, T., Isa, M.H., Mustafa, M.R.U., Yeek-Chia, H., Baloo, L., Manan, T.S.B.A. & Saeed, M.O. (2016). Cr(VI) adsorption from aqueous solution by an agricultural waste based carbon. *RSC Adv.* 6, 56365–56374. DOI: 10.1039/C6RA05618K.

8. Giraldo, L., Erto, A. & Moreno-Piraján, J.C. (2013). Magnetite nanoparticles for removal of heavy metals from aqueous solutions: synthesis and characterization. *Adsorption* 19(2), 465–474. DOI: 10.1007/s10450-012-9468–1.

9. Krishna, R.H. & Swamy, A. (2011). Kinetic and isotherm modeling of adsorption of Ni (II) form aqueous solutions onto powder of papaya seeds. *Int. J. Sci. Res. Publ.* 1(1), 1–6. ISSN 2250-3153.

10. Sanciolo, P., Harding, I.H. & Mainwaring, D.E. (1992). The Removal of chromium, nickel, and zinc from electroplating wastewater by adsorbing colloid flotation with a sodium dodecylsulfate/dodecanoic acid mixture. *Sep. Sci. Technol.* 27, 375–388. DOI: 10.1080/01496399208018887.

11. Murthy, Z.V.P. & Chaudhari, L.B. (2008). Application of nanofiltration for the rejection of nickel ions from aqueous solutions and estimation of membrane transport parameters. *J. Hazard. Mater.* 160, 70–77. DOI: 10.1016/j.jhazmat.2008.02.085.

12. Siboni, M.S., Samadi, M.T., Yang, J.K. & Lee, S.M. (2012). Photocatalytic removal of Cr(VI) and Ni(II) by UV/TiO₂: kinetic study. *Desalin. Water Treat.* 40, 77–83. DOI: 10.1080/19443994.2012.671144.

13. Chen, X., Huang, G. & Wang, J. (2013). Electrochemical reduction/oxidation in the treatment of heavy metal wastewater. *J. Metall. Eng.* 2, 161–164.

14. Dabrowski, A., Hubicki, Z., Podkościelny, P. & Robens, E. (2004). Selective removal of the heavy metal ions from waters and industrial wastewaters by ion-exchange method. *Chemosphere* 56, 91–106. DOI: 10.1016/j.chemosphere.2004.03.006.

15. Molinari, R., Poerio, T. & Argurio, P. (2008). Selective separation of copper(II) and nickel(II) from aqueous media using the complexationeultrafiltration process. *Chemosphere* 70, 341–348. DOI: 10.1016/j.chemosphere.2007.07.041.

16. Lakshtanov, L.Z. & Stipp, S.L.S. (2007). Experimental study of nickel(II) interaction with calcite: adsorption and coprecipitation. *Geochim. Cosmochim. Acta* 71, 3686–3697. http://dx.doi.org/10.1016/j.gca.2007.04.006.

17. Al-Asheh, S., Banat, F. & Mobai, F. (1999). Sorption of copper and nickel by spent animal bones. *Chemosphere* 39(12), 2087–2096. DOI: 10.1016/S0045-6535(99)00098-3.

18. Vijayaraghavan, K., Jegan, J., Palanivelu, K. & Velan, M. (2004). Removal of nickel(II) ions from aqueous solution using crab shell particles in a packed bed up-flow column. *J. Hazard. Mater.* B113, 223–230. DOI: 10.1016/j.jhazmat.2004.06.014.

19. Vijayaraghavan, K., Jegan, J., Palanivelu, K. & Velan, M. (2005). Biosorption of cobalt(II) and nickel(II) by seaweeds: batch and column studies. *Sep. Purif. Technol.* 44, 53–59. DOI: 10.1016/j.seppur.2004.12.003.

20. Panneerselvam, P., Morad, N. & Tan, K.A. (2011). Magnetic nanoparticle (Fe₃O₄) impregnated onto tea waste for the removal of nickel(II) from aqueous solution. *J. Hazard. Mater.* 186, 160–168. DOI: 10.1016/j.jhazmat.2010.10.102.

21. Hasar, H. (2003). Adsorption of nickel(II) from aqueous solution onto activated carbon prepared from almond husk. *J. Hazard. Mater.* 97, 49–57. DOI: 10.1016/s0304-3894(02)00237-6.

22. Fiol, N., Villaescusa, I., Martinez, M., Miralles, N., Poch, J. & Serarols, J. (2006). Sorption of Pb(II), Ni(II), Cu(II) and Cd(II) from aqueous solution by olive stone waste. *Sep. Purif. Technol.* 50, 132–140. DOI: 10.1016/j.seppur.2005.11.016.

23. Rao, M., Parwate, A.V. & Bhole, A.G. (2002). Removal of Cr⁶⁺ and Ni²⁺ from aqueous solution using bagasse and fly ash. *Waste Manage.* 22, 821–830. DOI: 10.1016/S0956-053X(02)00011-9.

24. Otun, J.A, Oke, I.A., Olarinoye, N.O., Adie, D.B. & Okuofu, C.A. (2006). Adsorption isotherms of Pb(II), Ni(II) and Cd(II) ions onto PES. *J. Appl. Sci.* 6(11), 2368–2376.

25. Olayinka, O.K., Oyedeji, O.A. & Oyeyiola, O.A. (2009). Removal of chromium and nickel ions from aqueous solution by adsorption on modified coconut husk. *Afr. J. Environ. Sci. Technol.* 3(10), 286–293. DOI: 10.5897/AJEST09.053.

26. Gao, Z., Bandosz, T.J., Zhao, Z., Han, M. & Qiu, J. (2009). Investigation of factors affecting adsorption of transition metals on oxidized carbon nanotubes. *J. Hazard. Mater.* 167, 357–365. DOI: 10.1016/j.jhazmat.2009.01.050.

27. Kandah, M.I. & Meunier, J.L. (2007). Removal of nickel ions from water by multi-walled carbon nanotubes. *J. Hazard. Mater.* 146(1-2), 283–288. DOI: 10.1016/j.jhazmat.2006.12.019.

28. Yang, S., Li, J., Shao, D., Hu, J. & Wang, X. (2009). Adsorption of Ni(II) on oxidized multi-walled carbon nanotubes: Effect of contact time, pH, foreign ions and PAA. *J. Hazard. Mater.* 166, 109–116. DOI: 10.1016/j.jhazmat.2008.11.003.

29. Chen, C., Hu, J., Shao, D., Li, J. & Wang, X. (2009). Adsorption behavior of multiwall carbon nanotube/iron oxide magnetic composites for Ni(II) and Sr(II). *J. Hazard. Mater.* 164, 923–928. DOI: 10.1016/j.jhazmat.2008.08.089.

30. Wu, S., Huang, J., Zhuo, C., Zhang, F., Sheng, W. & Zhu, M. (2016). One-Step Fabrication of Magnetic Carbon Nanocomposite as Adsorbent for Removal of Methylene Blue. *J. Inorg. Organomet. Polym. Mater.* 26(3), 632–639. DOI: 10.1007/s10904-016-0355–1.

31. He, F., Fan, J., Ma, D., Zhang, L., Leung, C. & Chan, H.L. (2010). The attachment of Fe₃O₄ nanoparticles to graphene oxide by covalent bonding. *Carbon* 48(11), 3139–3144. DOI: 10.1016/j.carbon.2010.04.052.

32. Hao, Y., Wang, Z., Gou, J. & Dong, S. (2015). Highly efficient adsorption and removal of Chrysoidine Y from aqueous solution by magnetic graphene oxide nanocomposite. *Arabian J. Chem.* http://dx.doi.org/10.1016/j.arabjc.2015.07.01.

33. Qu, S., Huang, F., Yu, S., Chen, G. & Kong, J. (2008). Magnetic removal of dyes from aqueous solution using multi-walled carbon nanotubes filled with Fe₂O₃ particles. *J. Hazard. Mater.* 160, 643–647. DOI: 10.1016/j.jhazmat.2008.03.037.

34. Zhu, J., Guo, H.G.J., Chen, M., Wei, H., Luo, Z., Colorado, H.A., Yerra, N., Ding, D., Ho, T.C., Haldolaarachige, N., Hopper, J., Young, D.P., Guo, Z. & Wei, S. (2014). Mesoporous magnetic carbon nanocomposite fabrics for highly efficient Cr(VI) removal. *J. Mater. Chem. A* 2, 2256–2265. DOI: 10.1039/C3TA13957C.

35. Pełech, I. (2010). Preparation of carbon nanotubes using CVD method. *Pol. J. Chem. Technol.* 12(3), 45–49. DOI: 10.2478/v10026-010-0033-y.

36. Sykuła-Zając, A., Turek, M., Mathew, M.P., Patai, F., Horvat, M. & Jabłońska, J. (2010). Determination of nickel in tea by using dimethylglyoxime method. Scientific Bulletin of the Technical University of Lodz. Food Chemistry and Biotechnology 74(1081), 5–11.

37. Li, H., Zhao, N., He, C., Shi, C., Du, X. & Li, J. (2008). Low temperature fabrication of hollow carbon nanospheres over Ni/Al₂O₃ by the catalytic method. *J. Alloys Comp.* 465, 387–390. DOI: 10.1016/j.jallcom.2007.10.090.

38. Canete-Rosales, P., Ortega, V., Álvarez-Lueje, A., Bollo, S., González, M., Ansón, A. & Martínez, M.T. (2012). Influence of size and oxidative treatments of multi-walled carbon nanotubes on their electrocatalytic properties. *Electrochim. Acta* 62, 163–171. DOI: 10.1016/j.electacta.2011.12.043.

39. Kolacyak, D., Ihde, J., Merten, C., Hartwig, A. & Lommatzsch, U. (2011). Fast functionalization of multi-walled carbon nanotubes by an atmospheric pressure plasma jet. *J. Coll. Inter. Sci.* 359, 311–317. DOI: 10.1016/j.jcis.2011.03.069.

40. Estévez-Martínez, Y., Velasco-Santos, C., Martínez-Hernández, A.L., Delgado, G., Cuevas-Yáñez, E., Alaníz-Lum-

breras, D., Duron-Torres, S. & Castaño, V.M. (2013). Grafting of Multiwalled Carbon Nanotubes with Chicken Feather Keratin. *J Nanomat.* 2013, 1–9. DOI: 10.1155/2013/702157.

41. Coates, J.P. (2000). *A Practical Approach to the Interpretation of Infrared Spectra. Encyclopedia of Analytical Chemistry.* John Wiley & Sons Ltd., Chichester.

42. Chen, J., Chen, Q., Ma, Q., Li, Y. & Zhu, Z. (2012). Chemical treatment of CNTs in acidic $KMnO_4$ solution and promoting effects on the corresponding Pd–Pt/CNTs catalyst. *J. Mol. Catal. A: Chem.* 356, 114–120. DOI: 10.1016/j.molcata.2011.12.032.

43. Helminiak, A., Mijowska, E. & Arabczyk, W. (2013). Characterization of carbon deposit with controlled carburization degree. *Mater. Sci. Pol.* 31(1), 29–35. DOI: 10.2478/s13536-012-0063-7.

44. Chairat, M., Rattanaphani, S., Bremner, J.B. & Rattanaphani, V. (2008). Adsorption kinetic study of lac dyeing on cotton. *Dyes Pigm.* 76, 435–439. DOI: 10.1016/j.dyepig.2006.09.008.

45. Kumar, P.S. & Kirthika, K. (2009). Equilibrium and kinetic study of adsorption of nickel from aqueous solution onto bael tree leaf powder. *J. Eng. Sci. Technol.* 4(4), 351–363.

46. Ai, L., Zhou, Y. & Jiang, J. (2011). Removal of methylene blue from aqueous solution by montmorillonite/$CoFe_2O_4$ composite with magnetic separation performance. *Desalination* 266, 72–77. DOI: 10.1016/j.desal.2010.08.004.

47. Kapoor, A. & Viraragavan, T. (1998). Heavy metal biosorption sites in Aspergillus Niger. *Bioresour. Technol.* 61, 221–227. DOI: 10.1016/S0960-8524(97) 00055-2.

48. Suemitsu, R., Uenishi, R., Akashi, I. & Kakano, M. (1986). The use of dyestuff-treated rice hulls for removal of heavy metals from wastewater. *J. Appl. Polym. Sci.* 31, 75–83. DOI: 10.1002/app.1986.070310108.

49. Al-Rub, F.A.A., Kandah, M. & Aldabaibeh, N. (2002). Nickel removal from aqueous solution by using sheep Manure Waste. *Eng. Life Sci.* 2, 111–116. DOI: 10.1002/1618-2863(200204).

50. Padmavathy, V. (2008). Biosorption of Ni(II) ions on Baker's yeast: kinetic, thermodynamic and desorption studies. *Bioresour. Technol.* 99, 3100–3109. DOI: 10.1016/j.biortech.2007.05.070.

51. Ho, Y.S., Jhonwase, D.A. & Forster, C.F. (1995). Batch nickel removal from aqueous solution by Sphagnum moss peat. *Water Res.* 29, 1327–1332. DOI: 10.1016/0043–1354(94)00236-3.

52. Ewecharoen, A., Thiravetyan, P. & Nakbanpote, W. (2008). Comparison of nickel adsorption form electroplating rinse water by coir pith and modified coir pith. *Chem. Eng. J.* 137, 181–188. DOI: 10.1016/j.cej.2007.04.007.

53. Huang, C., Ying-Chien, C. & Ming-Ren, L. (1996). Adsorption of Cu(II) and Ni(II) by palletized biopolimer. *J. Hazard. Mater.* 45, 265–267. DOI: 10.1016/0304-3894(95)00096-8.

54. Sharma, Y.C. & Srivastava, V. (2010). Separation of Ni(II) ions from aqueous solutions by magnetic nanoparticles. *J. Chem. Eng. Data* 55, 1441–1442. DOI: 10.1021/je900619d.

55. Meena, A.K., Mishra, G.K., Rai, P.K., Rajgopal, C. & Nagar, P.N. (2005). Removal of heavy metal ions from aqueous solution using carbon aerogel as an adsorbent. *J. Hazard. Mater.* 122, 161–170. DOI: 10.1016/j.jhazmat.2005.03.024.

56. Johnson, C.D. & Worrall, F. (2007). Novel granular materials with microcrystalline active surfaces-waste water treatment applications of zeolite/vermiculite composites. *Water Res.* 41, 2229–2235. DOI: 10.1016/j.watres.2007.01.047.

57. Kinhikar, V.R. (2012). Removal of Nickel (II) from Aqueous Solutions by Adsorption with Granular Activated Carbon (GAC). *Res. J. Chem. Sci.* 2(6), 6–11. ISSN 2231-606X.

58. Yueming Ren, N.Y. (2011). Graphene/δ-MnO 2 composite as adsorbent for the removal of nickel ions from wastewater. *Chem. Eng. J.* 175, 1–7. DOI: 10.1016/j.cej.2010.08.010.

59. Jha, V.K., Matsuda, M. & Miyake, M. (2008). Sorption properties of the activated carbon-zeolite composite prepared from coal fly ash for Ni^{2+}, Cu^{2+}, Cd^{2+} and Pb^{2+}. *J. Hazard. Mater.* 160, 148–153. DOI: 10.1016/j.jhazmat.2008.02.107.

60. Thamilarasu,P., Sivakumar, P. & Karunakaran, K. (2011). Removal of Ni(II) from aqueous solutions by adsorption onto Cajanus cajan L Milsp seed shell activated carbons. *Indian J. Chem. Technol.* 18(5), 414–420.

61. Zhang, X. & Wang, X. (2015). Adsorption and desorption of nickel(II) ions from aqueous solution by a lignocellulose/montmorillonite nanocomposite. *PLoS One* 10, e0117077. DOI: 10.1371/journal.pone.0117077.

62. Karagoz, S., Tay, T., Ucar, S. & Erdem, M. (2008). Activated carbons from waste biomass by sulfuric acid activation and their use on methylene blue adsorption. *Bioresour. Technol.* 99, 6214–6222. DOI: 10.1016/j.biortech.2007.12.019.

63. Kara, M., Yuzer, H., Sabah, E. & Celik, M.S. (2003). Adsorption of cobalt from aqueous solutions onto sepiolite. *Water Res.* 37, 224–232. DOI: 10.1016/S0043–1354(02)00265-8.

64. Jaycock, M.J. & Parfitt, G.D. (1981). *Chemistry of Interfaces.* Ellis Horwood Ltd., Onichester.